J Mater Sci (2009) 44:2907–2915
DOI 10.1007/s10853-009-3384-0

Photoelectrochemical behavior of titania nanotube array grown on nanocrystalline titanium

Yibing Xie · Limin Zhou · Jian Lu

Received: 25 December 2008 / Accepted: 4 March 2009 / Published online: 25 March 2009

Abstract Surface nanocrystallization of titanium metal is processed by a high-energy shot peening treatment for drastic subdivision of bulk crystalline grains. Titania nanotube array directly grown on the nanocrystalline titanium substrate is achieved by a controlled anodization process. Field emission scanning electron microscopy, X-ray diffraction, and impedance spectroscopy analysis are conducted to investigate surface morphology, crystal phase, and electrical conductivity, respectively. The photoelectrochemical performance of the tailored titania nanotubes/titanium nanocrystallites has been investigated under UV light illumination. When the microstructure of the titanium substrate is modified from bulk crystals to nanocrystallites, the obtained titania nanotube array exhibits an independent structure with enlarged pore size and thinned tube wall, which is ascribed to the intensified anodic oxidation of ultrafine titanium crystallites along intergranular boundaries. Owing to the promoted interfacial electron transfer of the titania/nanocrystalline titanium, the complex impedance predominated by the charge transfer resistance has been significantly decreased in the electrochemical process. Both photocurrent and photovoltage responses have accordingly enhanced as well in the photoelectrochemical process.

Y. Xie (✉)
School of Chemistry and Chemical Engineering,
Southeast University, Nanjing, China
e-mail: ybxie@seu.edu.cn

L. Zhou · J. Lu
Department of Mechanical Engineering, The Hong Kong
Polytechnic University, Kowloon, Hong Kong, China

Introduction

Titania (TiO_2) semiconductor, as one of the important photoactive materials, has many potential applications, such as photocatalytic degradation of environmental pollutants, photocatalytic synthesis of organic compounds, photoelectric conversion of solar energy, and even photonic crystals. Many methods have been used to fabricate TiO_2 with various structures such as synthetic single crystals, multiporous films, and micro- or nano-particles [1]. The porous geometries are typically preferred as they provide a high surface area, which leads to an improvement of photoreaction efficiency. Concerning the microstructure of TiO_2 film electrodes, random arrangement of nanoparticles usually results in limited active areas, because only external surface in the outside layer of TiO_2 compact film can take effect. Insufficient scattering of light becomes another problem because the diameter size of nanoparticles is much smaller than the wavelength of UV and visible lights [2, 3]. The weak bonding strength between TiO_2 layer and conductive substrates (such as indium tin oxide and fluorine-doped tin oxide) can also inhibit interfacial electron transfer, which finally influences photoresponse efficiency [4]. So, microstructure modification of TiO_2 crystallites becomes highly required to improve the photoelectrochemical performance [5]. One of the effective ways is to tailor TiO_2 layer from ordinary porous structure to the aligned nanotubes, nanorods, nanoribbons, or nanowires, since these highly oriented nanostructures contribute to a better light harvesting and electron transportation than their particulate forms [6, 7]. In addition, microstructure modification of electrode substrate is another approach to optimize the composite electrode because the electronic properties are much related to the interfacial connection between titania layer and its substrate [6, 8]. Recent research studies report that grain refinement

of the surface layer of metal or alloy materials can be well achieved by the surface mechanical attrition treatment [9, 10]. Especially for titanium metal, the intrinsic properties can be fully modified through the surface nanocrystallization process [11, 12]. As a versatile functional material of titania/titanium composite, the nano-textured titanium oxide with a porous structure has been successfully synthesized by either a controlled chemical oxidation of bare titanium metal or a continuous anodization of nanoimprinted titanium metal [13, 14]. Moreover, TiO_2 nanotubes can be well fabricated from bulk crystalline titanium metal by a controlled potentiostatic anodization process [15–18]. For the purpose of improving the overall photoactivity, the pretreated metallic titanium sheet has been used as a precursor to prepare titania/titanium (TiO_2/Ti) composite electrode.

In this study, microstructure modification of both oxide layer and metal substrate has been adopted to fabricate TiO_2/Ti nanocomposite. A high-energy shot peening process is initially executed for surface nanocrystallization of Ti metal sheet. Anodic oxidation process is then followed to form TiO_2 nanotube array on the surface of nanocrystalline Ti substrate. Photoelectrochemical performances are also investigated to explore potential applications of such an integrated nanocomposite.

Experimental

Materials

Titanium sheet (Ti, purity >99.6%, thickness 0.5 mm) was purchased from Goodfellow Cambridge Ltd. All chemical reagents were analytical grade and purchased from Sigma-Aldrich Co. Doubly distilled water was used throughout the whole experiment. All electrochemical and photoelectrochemical measurements were carried out in a 0.1-M phosphate buffered saline (PBS) electrolyte solution with a pH of 6.8.

Preparation of TiO_2/Ti

The first process is to prepare a nanocrystalline layer on the surface of bulk crystalline Ti metal. A high-energy shot peening process driven by a 20-kHz ultrasonic generator was carried out in a vacuum condition for 5 min at room temperature. The second process is to fabricate TiO_2 nanotube array based on this nanocrystalline Ti substrate. The pretreated Ti sheet was ultrasonically cleaned in alcohol and acetone solution for 20 min and then chemically polished in a concentrated hydrofluoride acid/nitric acid solution for 8 s to form a fresh metal surface. An anodic oxidation process was followed in an electrochemical cell by using this Ti sheet as an anode, Pt foil as a cathode, and H_3PO_4 (0.5 M)–HF (0.2 M) aqueous solution as an electrolyte. A potentiodynamic anodization was initially carried out to form an ultra thin layer of titania oxide when the anodizing voltage was continuously increased from 0 to 20 V. The following potentiostatic anodization was maintained at 20 V and the whole electrochemical reaction time was 40 min. After that, as-prepared TiO_2/Ti sample was adequately washed with deionized water and dried in an oven at 378 K for 24 h. A post-treatment of calcination process was then conducted at 723 K for 2 h to achieve a phase transition of TiO_2 product. As a comparison experiment, all the same processes were also conducted to prepare TiO_2/Ti sample on the basis of an original bulk crystalline Ti sheet without any high-energy shot peening pre-treatment.

Characterization and analytical methods

Field emission scanning electron microscopy (FESEM, JEOL JSM-6335F) was used to investigate surface morphology and microstructure. To determine the crystal phase behaviors, X-ray diffraction (XRD, Philips PW3020) experiments were carried out on an X-ray diffractometer fitted with a graphite monochromator. To evaluate electrochemical and photoelectrochemical behaviors, an electrochemical workstation (CHI660C, CH Instruments, Inc.) was applied for linear sweep voltammetry, photocurrent, and photovoltage measurements. Electrochemical impedance spectroscopy (EIS, IM6e, ZAHNER elektrik, Germany) has also been used to investigate interfacial electron transfer process.

Experimental setup and procedures

Photoelectrochemical experimental system was set up in a cylindrical quartz cell by using an electrochemical workstation with a standard three-electrode configuration. TiO_2/Ti composites were used as the working electrodes with an effective area of 1.0 cm^2, a standard Hg/Hg_2Cl_2 saturated calomel electrode (SCE) as a reference electrode and Pt foil as a counter electrode. The photocurrent and photovoltage responses of TiO_2/Ti composites were measured in 0.1 M PBS electrolyte. A UV light source, having main wavelength of 365 nm and average intensity of 0.267 mW cm^{-2}, was used to irradiate TiO_2/Ti composite electrodes.

Results and discussion

Microstructural characterization

FESEM characterization has been conducted to examine the surface morphologies of Ti substrates and TiO_2/Ti

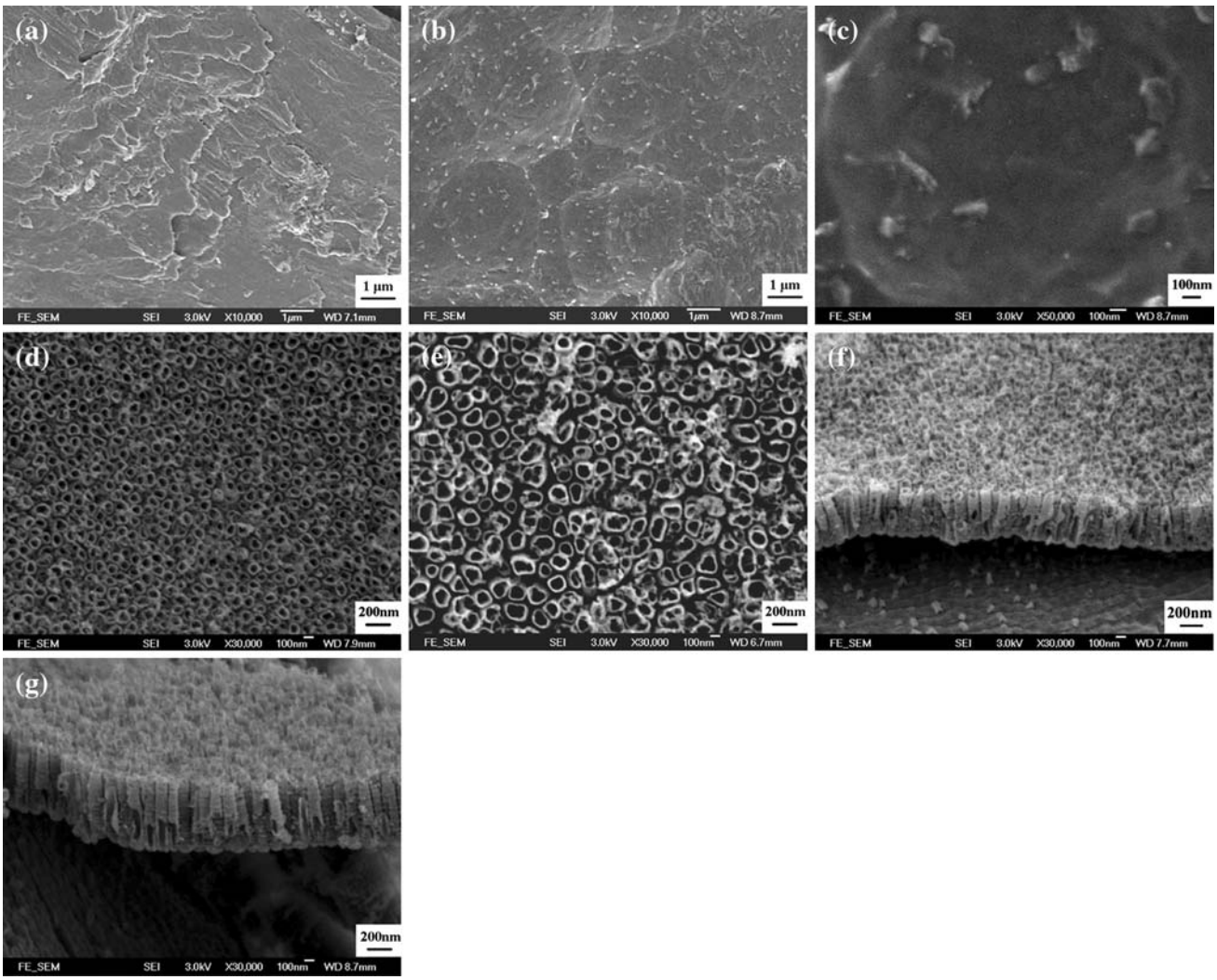

Fig. 1 Top-view FESEM images of **a** bulk crystalline Ti and **b** nanocrystalline Ti; enlarged view FESEM images of **c** nanocrystalline Ti, **d** TiO_2 on bulk crystalline Ti, and **e** TiO_2 on nanocrystalline Ti; cross-sectional view FESEM images of **f** TiO_2 on bulk crystalline Ti and **g** TiO_2 on nanocrystalline Ti

composites. Their images are shown in Fig. 1. Original bare Ti sheet has a rough surface with a coarse-grained bulk crystalline structure. However, after a high-energy shot peening treatment, the surface indentions are clearly appeared due to the high-flux bombardment of microballs. The corresponding surface crystal layer can be well subdivided into many pieces of ultrafine grains, whose individual crystallite size is approximately in the range of 100 nm (see Fig. 1a–c). A severe plastic deformation caused by the ultrasonic bombarding treatment has generated high strain strength at the crystalline boundaries and meanwhile accompanied by a dislocation slip, which finally leads to the subdivision of Ti metallic crystals from original coarse grains to nanometer- or submicron-sized grains in the top layer [19, 20]. So, the high-energy shot peening process can effectively promote the grain refinement, which ultimately results in the nanocrystallization on the surface of Ti sheet. Regarding the anodization process in acidic fluoride electrolyte, highly ordered TiO_2 nanotubes with a vertical orientation and unique open-mouth structure have been well synthesized on the basis of both Ti metal substrates. TiO_2 nanotubes made from bulk crystalline Ti have the inner diameter of 60 nm and the wall thickness of 15 nm in an average. Comparatively, the corresponding size has been tailored to a larger inner diameter of about 80–100 nm and a thinner wall thickness of about 12 nm for TiO_2 nanotubes made from nanocrystalline Ti. Moreover, the obtained TiO_2 nanotubes on nanocrystalline Ti substrate are separated from each other and show a more independent structure, which is very different from the wall-interconnected TiO_2 nanotubes grown on bulk crystalline Ti (see Fig. 1d, e). So, the corresponding inter-tube distance of TiO_2 nanotube array grown on nanocrystalline Ti substrate is larger than that on

bulk crystalline Ti substrate. However, as-prepared TiO_2 layers on both bulk crystalline Ti and nanocrystalline Ti have a similar tube length of approximately 500–520 nm (see Fig. 1f, g). In general, the electrochemical anodization of Ti metal at a voltage of 20 to 30 V in aqueous acidic fluoride solution can produce TiO_2 nanotubes with a constant height and pore size. Herein, owing to an increase in the activated interface area through subdividing Ti crystallites, the electrochemical oxidation reaction can be boosted for nanocrystalline Ti substrate than that for bulk crystalline Ti substrate. On the other hand, the chemical corrosion dissolution reaction is similar for both kinds of TiO_2, which is mostly dependent on fluorine ion concentration and pH value of electrolyte. Accordingly, the intensified electro-oxidation reaction along intergranular boundaries at a radial direction of tubes can contribute the formation of independent arrangement of these TiO_2 nanotubes with the separated tubes and thinned walls. However, the field-assisted anodization and dissolution reaction at an axial direction is highly dependent on the anodizing voltage and electrolyte component. Therefore the final length of TiO_2 nanotubes still keeps a constant value of approximately 500 nm for both Ti substrates, which is mainly decided by the electrochemical corrosion rate in the steady growth stage.

XRD analysis

In order to investigate the crystal structure of Ti substrates and TiO_2/Ti nanocomposites, XRD measurements have been carried out and the corresponding patterns are shown in Fig. 2. In view of characteristic diffraction peaks of titanium metal (see curves a and b), both Ti substrates demonstrate a complete crystallization structure no matter whether they conduct the high-energy shot peening treatment or not. Comparatively, nanocrystalline Ti has stronger diffraction peaks than bulk crystalline Ti at $2\theta = 38.5$ and 40.2°. It means the subdivision of bulk crystalline Ti metal caused by the high-energy shot peening treatment can effectively improve its crystalline quality and integrality. Additionally, according to the appearance of characteristic diffraction peaks at $2\theta = 25.4$ and 48.1° for *hkl*(101) and *hkl*(200) crystal lattice planes, both kinds of TiO_2/Ti nanocomposites exhibit the same crystal phase of anatase TiO_2 (see curves c and d). Although the morphologies of as-prepared TiO_2 nanotubes are highly related to the crystal microstructure of Ti substrates, the chemical product of TiO_2 synthesized in an anodization process must be identical for both kinds of Ti substrates. It should be noted that the anodic oxidation at 20 V only results in the formation of amorphous TiO_2, because such an anodizing voltage is far below the critical sparking discharge voltage of 100 V to achieve a direct crystallization for as-prepared TiO_2 [21]. The post-treatment of calcination process at 723 K becomes a necessary procedure for the crystallization of TiO_2. In view of characteristic diffraction peaks of TiO_2 observed in XRD patterns, the phase transition from amorphous to anatase is identical to achieve a complete crystallization through the heating treatment for both kinds of TiO_2 products. The different intensities of these characteristic diffraction peaks are ascribed to TiO_2 nanotube layer thickness. As a result, the crystallinity of TiO_2 nanotube layer grown on both kinds of Ti substrates is very similar.

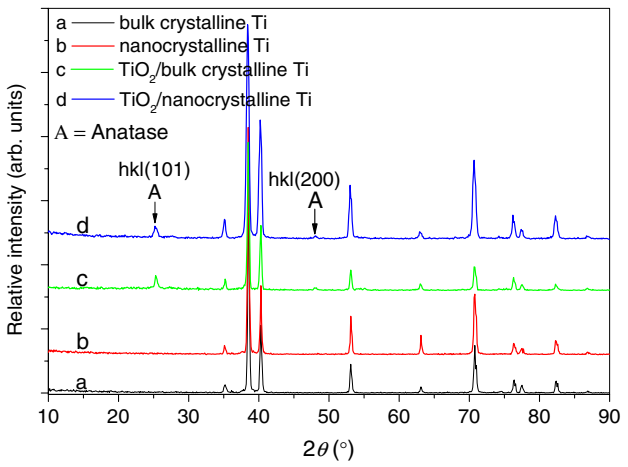

Fig. 2 XRD patterns of two kinds of Ti substrates and TiO_2/Ti nanotube composites

Electrochemical properties

The whole anodization process of two Ti metal sheets can be divided into three stages, whose current–time curves are shown in Fig. 3. In the stage I, the electrochemical current soars quickly up to the peak value in a short time, which is due to the drastic electro-oxidation of fresh Ti metal. Then, this current sharply declines down to a low value, which is ascribed to the formation of compact oxide layer on Ti substrate. In the stage II, the anodic current begins to rise again up to a high value, which is due to the intensified electrochemical corrosion reaction of as-formed titanium oxide. Then, this anodic current conducts an obvious decay to a lower level, which is due to the continuous increase in electrical resistance caused by an accumulation of titanium oxide since the anodic oxidation process becomes a predominant process. In the stage III, the anodic current gradually approaches to a constant value. The dissolving rate must have been close to the producing rate of titanium oxide, which leads to forming uniform nanotubes with a constant length. Usually, the microstructure of TiO_2 layer is mostly dependent on the anodizing voltage and electrolyte component, which will essentially determine the

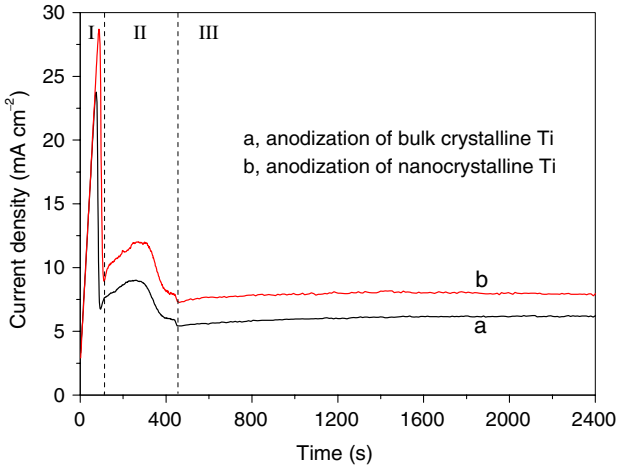

Fig. 3 Anodized oxidation curves of two kinds of Ti metals in HF–H_3PO_4 aqueous electrolyte

reaction rate of electrochemical oxidation and chemical corrosion [22]. A stable potentiostatic anodization process at 20 V is applied for the subsequent electrochemical synthesis reaction after a fluctuation of the anodizing voltage during an initial potentiodynamic anodization process. The oxide barrier layer would suffer the cyclic breakdown and regeneration to form random pits on the surface layer, which can be well tailored to a tubular structure. Such a formation mechanism is related to a dynamic equilibrium process between the anodic oxidation of Ti ($Ti + 2H_2O - 4e^- \rightarrow TiO^{2+} + 2H^+$; $TiO^{2+} + H_2O \rightarrow TiO_2 + 2H^+$) and corrosion dissolution of TiO_2 ($TiO_2 + 6HF \rightarrow [TiF_6]^{2-} + 2H_2O + 2H^+$; $TiO_2 + H_2O + H^+ \rightarrow [Ti(OH)_3]^+$) [23, 24].

Comparatively, the average anodization current of nanocrystalline Ti is much higher than that of bulk crystalline Ti in a steady growth stage. Such a difference of anodization current is highly associated with the crystalline structure of Ti substrates. Surface nanocrystallization leads to a severe decrease in grain size from tens of micrometer for bulk crystalline Ti to a nanoscale for nanocrystalline Ti, which can intensively enhance the interfacial grain area and surface energy as well [20]. Such Ti nanocrystallites have a very large intercrystalline area and residual stress. Usually, the interfacial energy of intercrystalline atoms is much higher than that of inner atoms for individual crystallite due to the quantum size effect [25]. Accordingly, the activated intercrystalline Ti atoms can conduct an intensified electrochemical oxidation reaction at intergranular boundaries. So, the electrochemical current response of nanocrystalline Ti is much higher than that of bulk crystalline Ti in the anodization process. Meanwhile, the chemical corrosion dissolution reaction rate is similar for both kinds of titanium oxides, which is mostly dependent on fluorine ion concentration and pH value of electrolyte. The obvious intensification of anodic oxidation reaction on nanocrystalline Ti leads to a more independent tubular structure of TiO_2 nanotubes, which eventually promotes a surface area increase.

In order to investigate the interfacial electrical conductivity of Ti substrate in an electrolyte solution, the complex impedance analysis has been carried out in a traditional three-electrode system. The electrochemical EIS measurements are conducted by applying a sinusoidal perturbation of ±5 mV, at a constant electrode potential of −0.4 V and over frequencies from 100,000 to 0.01 Hz. Along with a continuous increase in frequency, the electrode's complex impedance dramatically decreases at a low frequency below 300 Hz and then gradually reached a steady value at a frequency above 1000 Hz. The nanocrystalline Ti substrate obviously has a lower impedance value than bulk crystalline Ti in a high frequency range of 100 to 100,000 Hz although both of them exhibit very similar impedance values at a low frequency below 100 Hz (see Fig. 4a). In general, the complex impedance is composed of charge transfer resistance in series with mass transfer impedance containing linear and nonlinear diffusion terms. However, the semicircle characteristic in the corresponding Nyquist plots reveals that a kinetic behavior must have predominantly occurred for two kinds of Ti substrates in the electrochemical process (see Fig. 4b). An obvious descent of charge transfer resistance can also be observed and their values can be qualitatively determined by comparing the radiuses of curvatures. So, owing to the diminishing crystal size of nanocrystalline Ti, the activation of intercrystalline atoms can lead to an improvement of the electrical conductivity. This result is in high agreement with the enhancement of anodization current in the electrochemical oxidation of nanocrystalline Ti. Therefore, such a nanostructure of Ti substrate can benefit the interfacial electron transfer in the electrochemical and photoelectrochemical processes.

The impedances at a medium or high frequency are particularly important because they usually correspond to the characteristic frequency of molecular interaction potentials [26]. Both the frequency and electrode potential have been applied to investigate their influences on the complex impedance of TiO_2/Ti electrodes. Firstly, the complex impedance in terms of the applied electrode potential has been investigated for two kinds of nanotubular TiO_2/Ti composites, as shown in Fig. 5. Both complex impedances continuously decline until they appear a sharp falling when the electrode potential is swept from positive to negative position, which is attributed to the *n*-type semiconductor characteristic of TiO_2. The critical electrode potential range, corresponding to the significant variation of complex impedance, can be determined as 0 to −0.5 V for TiO_2/bulk crystalline Ti and 0.35

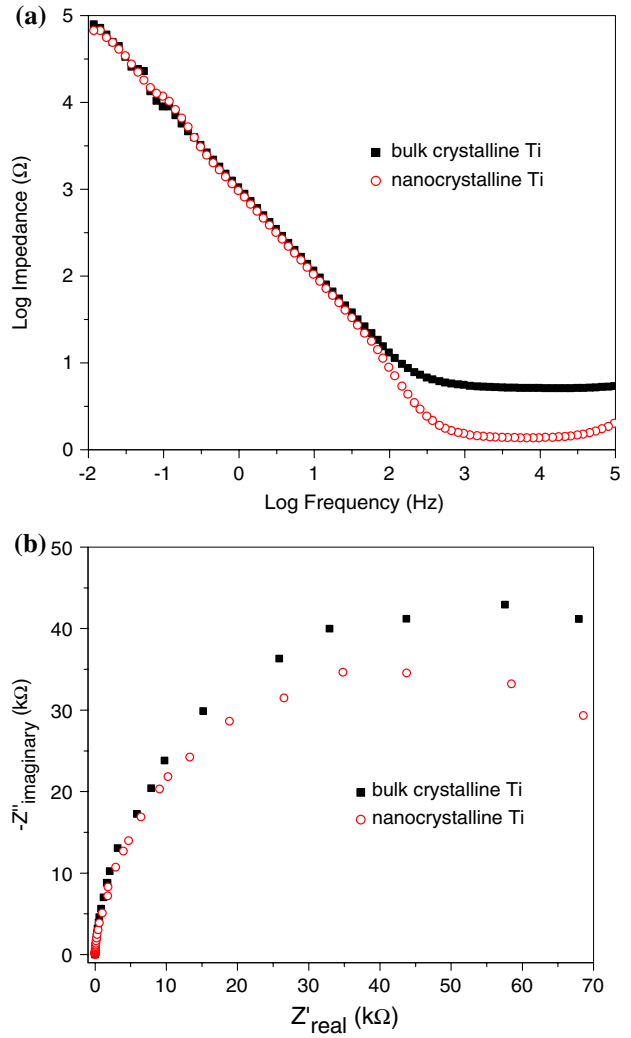

Fig. 4 **a** Bode plots and **b** Nyquist plots of bulk crystalline Ti and nanocrystalline Ti at a constant potential of −0.40 V vs. SCE in 0.1 M PBS solution

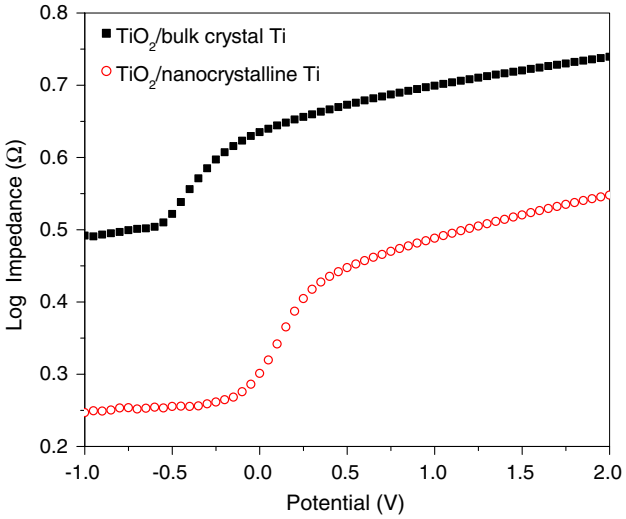

Fig. 5 Complex impedance response in terms of the applied electrode potential for two kinds of TiO_2/Ti nanotube composites in 0.1 M PBS electrolyte

to −0.15 V for TiO_2/nanocrystalline Ti, respectively. The threshold potential shifts toward a more positive position for TiO_2/nanocrystalline Ti, which is due to its thicker oxide barrier layer linking with TiO_2 and Ti. So, the applied electrode potential can considerably influence the complex impedance. Moreover, the impedance value of TiO_2/nanocrystalline Ti caused by the charge-transfer resistance is obviously lower than that of TiO_2/bulk crystalline Ti under the same electrode potential condition during the electrochemical process. As described above, the electrical conductivity of Ti substrates can be enhanced through the nanocrystallization process, which thus lowers charge-transfer resistance of TiO_2/Ti nanocomposite electrode.

EIS has also been applied to investigate the electrical conductivity of nanotubular TiO_2/Ti composite electrodes over the frequency from 100,000 to 0.01 Hz under a sinusoidal perturbation of ±5 mV and a constant potential of −0.4 V. Bode plots show that TiO_2/nanocrystalline Ti exhibits much lower impedance value than TiO_2/bulk crystalline Ti in the testing frequency range. Such a difference becomes more significant at a low frequency below 300 Hz (see Fig. 6a). The Nyquist plots usually presents a semicircle-like characteristic in its complex plane when the electrode impedance is predominantly determined by the charge transfer resistance in a kinetics-controlled process [27]. Herein, the proposed equivalent circuit, as shown in Fig. 7, has been applied to fit EIS experimental data obtained in the electrochemical process for TiO_2/Ti nanocomposite electrodes. The corresponding Nyquist plots are also shown in Fig. 6b. The fitting curves are presented as solid lines and the experimental data are denoted as individual symbols. In this circuit, the parallel combination of $R_{TiO_2/Ti}$ and C are associated with the electrical conductivity and capacitance of the TiO_2/Ti nanotube electrodes. The parallel combination of the interfacial charge transfer resistance $\left(R_{TiO_2/Ti-E}\right)$ and the constant phase element (CPE) could lead to a semicircle-like shape in the corresponding Nyquist impedance plots. Herein, CPE demonstrates the diffusion characteristics of the electrochemical system, which is defined by two parameters of CPE-T and CPE-P. CPE-T indicates the electrostatic capacitance of CPE element (unit, F). CPE-P is defined as an index indicating a degree of a deviation from a certain state (dimensionless unit). As a result, the fitting results of CPE-P are determined as 0.84 and 0.95 for two kinds of TiO_2/Ti electrodes, whose values are approximately close to 1.0. Thus, the CPE-T obtained in this study is similar to a capacitor element. Moreover, $R_{TiO_2/Ti}$, $\left(R_{TiO_2/Ti-E}\right)$ and C impedance components are obtained as 4272, 634 Ω, and

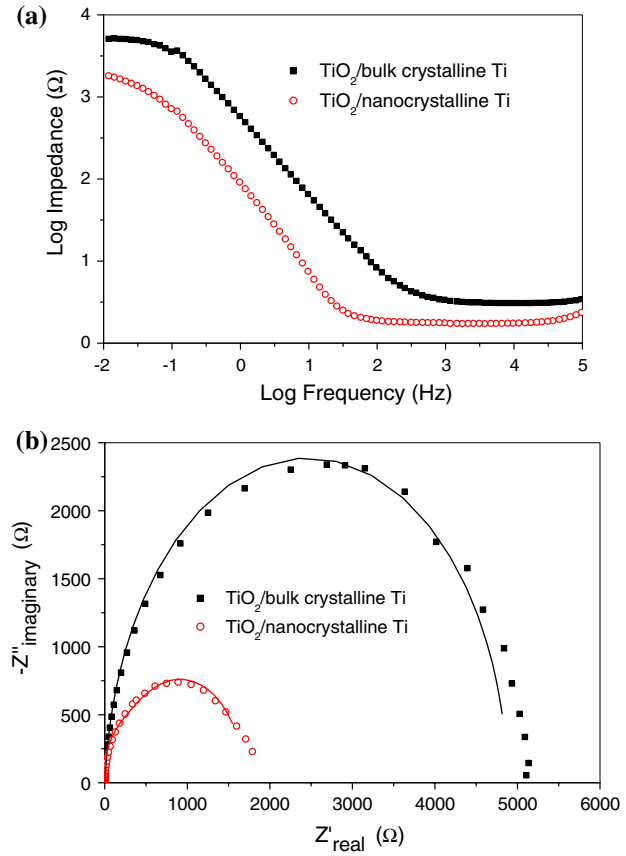

Fig. 6 **a** Bode plots and **b** Nyquist plots of two kinds of TiO_2/Ti nanotube composites in 0.1 M PBS electrolyte at a constant potential of −0.40 V vs. SCE (The *solid lines* are the fitting curves and the *denoted symbols* are experimental data in plot **b**)

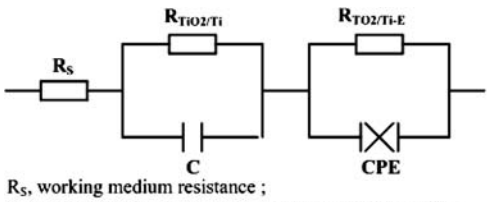

R_S, working medium resistance ;
$R_{TiO2/Ti}$, charge flow resistance across TiO_2/Ti electrode;
C, TiO_2 capacitance including surface-state and Helmholtz double layer;
$R_{TiO2/Ti-F}$, charge transfer resistance between TiO_2/Ti and Electrolyte interface;
CPE, constant phase element defined by CPE-T and CPE-P

Fig. 7 Schematic diagram of impedance equivalent circuit of TiO_2/Ti nanotube composites in the electrochemical process

0.38 mF for TiO_2/bulk crystalline Ti and 1455, 232 Ω, and 3.02 mF for TiO_2/nanocrystalline Ti. Obviously, the decrease in the charge flow resistance and interfacial charge transfer resistance, along with the increase in capacitance, are highly related to surface area and interfacial activity of TiO_2 layer and Ti substrate. Herein, the complex impedance is composed of dominant resistances of charge flow across TiO_2/Ti and TiO_2/electrolyte interfaces, subordinate resistances of electrolyte solution and Ti substrate, and capacitances of TiO_2 surface layer and Helmholtz double layer [28, 29]. Independent nanotube structure of TiO_2 with a higher surface area benefits the electron-diffusion transport at both sides of tube walls. At the same time, the nanocrystalline structure of Ti with a much smaller crystal size benefits the interfacial electron shift from TiO_2 layer to Ti substrate. The lower resistance and higher capacitance result in a better electrical conductivity for this nanotubular TiO_2/nanocrystalline Ti composite electrode. So, in a certain degree, the apparent impedance value can mostly reflect the total efficiency of electron transfer in the electrochemical process as well as that in the photoelectrochemical process (Table 1).

Photoelectrochemical properties

Both photocurrent and photovoltage responses are regarded as key parameters to characterize TiO_2 photoactivities and electronic properties in the photoelectrochemical process. Photoelectrochemical performances of two kinds of TiO_2/Ti electrodes differ greatly from each other, which are very dependent on their microstructure and geometry of both oxide films and metallic substrates [30]. To further study the photo-induced charge generation, separation, and electron transfer of TiO_2/Ti nanocomposites, the photoelectrochemical response measurements are conducted in 0.1 M PBS electrolyte under UV light illumination.

Linear sweep voltammetry analysis is firstly applied to examine the photoelectrochemical behaviors of TiO_2/Ti nanocomposites. The corresponding experimental results are shown in Fig. 8. Both TiO_2/Ti electrodes exhibit similar polarization current curves when the anodic potential is swept from 0 to 1 V vs. SCE under a dark condition. The polarization current responses are very insignificant for both electrodes in the electrochemical process as few charge carriers transport through *n*-type TiO_2 semiconductor. Comparatively, TiO_2 nanotubular layer on nanocrystalline Ti exhibits a higher polarization current than that on bulk crystalline Ti, owing to its lower physical electrical resistance. Under UV illumination condition, the anodic current responses have drastically enhanced for both electrodes. This current intensity can be further improved through increasing the anodic potential because the applied potential has already exceeded the flat-band potential of crystalline anatase TiO_2 (approximately −0.16 V vs. NHE at pH 0) [30]. The anodic potential applied on TiO_2/Ti electrode can positively drive those photo-induced electrons away from TiO_2 conduction band to form out-circuit current and ultimately promotes current intensity. It should be noted that this photoelectrochemical current response is mostly ascribed to photocurrent rather than sole electrochemical current because the applied

Table 1 Simulation parameters of equivalent circuits of nanotubular TiO_2/bulk crystalline Ti and TiO_2/nanocrystalline Ti

Nanotubular composite	Rs (Ω)	C (mF)	$R_{TiO_2/Ti}$ (Ω)	CPE-T	CPE-P	$(R_{TiO_2/Ti-E})$ (Ω)
TiO_2/bulk crystalline Ti	3.1	0.38	4272	0.0020	0.84	634
TiO_2/nanocrystalline Ti	1.8	3.02	1455	0.0037	0.95	232

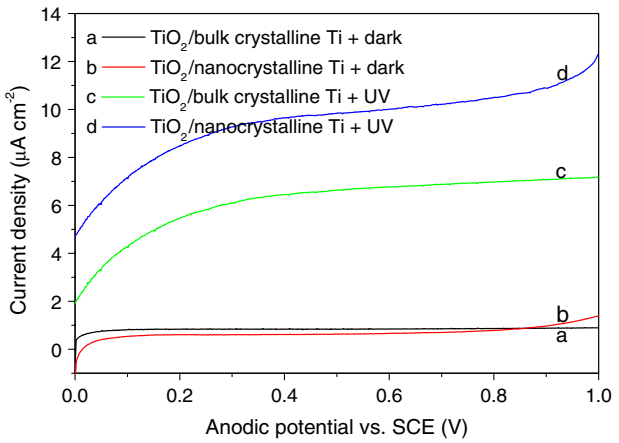

Fig. 8 Linear sweep voltammetry current curves of (a, c) TiO_2/bulk crystalline Ti and (b, d) TiO_2/nanocrystalline Ti nanotube composites with and without UV light illumination

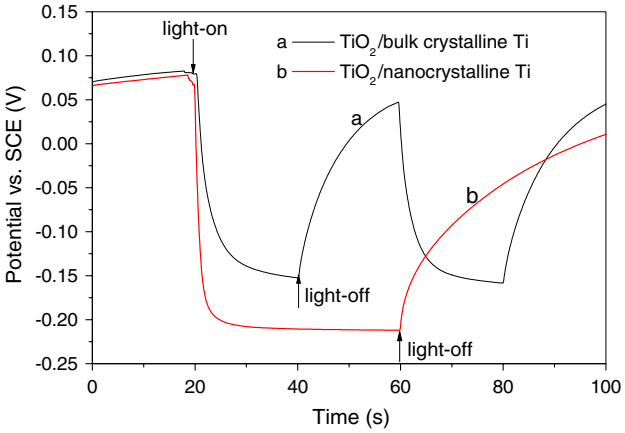

Fig. 9 Photovoltage curves of two kinds of TiO_2/Ti nanotube composites under UV light pulse illumination

anodic potential (0–1 V vs. SCE) is much below the critical potential (approximately 1.6 V vs. SCE) of an electro-oxidation reaction for water decomposition, which is due to the overpotential effect on TiO_2 nanotubes. Noticeably, at a higher anodic potential above 0.25 V for TiO_2/bulk crystalline Ti and 0.35 V for TiO_2/nanocrystalline Ti, a photoresponse plateau has been observed for both photoanodes, which might be ascribed to the geometrical limitation of TiO_2 nanotubes. For a tube shaped *n*-type TiO_2 semiconductor, the majority of charge carrier depletion zones is generated at both sides of the tube walls and the entire tube sidewalls consisted of the space charge layers [31]. The thickening space charge layer, caused mostly by an increase in the applied anodic potential, leads to a photocurrent promotion. Photocurrent saturation is theoretically achieved when the thickness of space charge layer is close to the tube wall thickness. Comparatively, a much higher current response is obtained under the same anodic potential for TiO_2/nanocrystalline Ti than that for TiO_2/bulk crystalline Ti. Such a difference of anodic photocurrent can be further magnified with an increase in the applied anodic potential. Considering the interconnected nanotube structure, the space charge layer could be probably squeezed due to the partially overlapped electric fields along the external sidewall. Besides that, the photocurrent responses, highly related to the total photoelectron density, are also dependent upon the active surface area of TiO_2. So, independent nanotube array structure can benefit the overall polarization current and photocurrent for TiO_2/Ti nanocomposite, because both side tube walls can act as photoelectrochemical reaction sites. Higher photocurrent response means more photo-induced electrons have been effectively transported from TiO_2/Ti photoanode to counter electrode through the external circuit.

UV light-induced photovoltage response of TiO_2/Ti nanocomposites has also measured and the corresponding experimental curves are shown in Fig. 9. It reveals that the potential is about 0.08 V vs. SCE for both TiO_2/Ti electrodes under a dark condition. In the case of UV light illumination, the electrode potential sharply declines until it reaches steady values of −0.153 V and −0.213 V vs. SCE, which are regarded as photopotentials of TiO_2/bulk crystalline Ti and TiO_2/nanocrystalline Ti, respectively. Herein, more negative value of photopotential means that more photo-induced electrons can effectively transfer to the conduction band of TiO_2. The photoelectron collection leads to forming a space charge layer on nanotube sidewalls, which eventually generates a photopotential response. When UV light is turned off, this potential gradually rises up to the initial value again. These electrons on the conduction band must have suffered a relaxation process through recombining with holes on the valence band, owing to a strong electric field distribution within the depletion layers. So, TiO_2/Ti nanocomposites can act well as a representative *n*-type semiconductor to conduct the transfer and decay of the excited-state photoelectrons under UV light pulse illumination. Comparatively, the photovoltage, defined as the UV light illumination-induced change of the electrode potential,

has enhanced from 0.233 V for TiO_2/bulk crystalline Ti to 0.291 V for TiO_2/nanocrystalline Ti. This experimental result highly agrees with the above photocurrent measurement outcome. It means that the photoelectron collection efficiency can be improved for these featheredged TiO_2 nanotubes with an independent arrangement. It is noteworthy that microstructure modification of Ti substrate from bulk crystalline to nanocrystallites is able to effectively trigger interfacial electron shift, which eventually leads to a more significant promotion of photocurrent rather than photovoltage for TiO_2/Ti photoanodes. Such a difference of photocurrent and photovoltage reflects the overall photoelectron efficiency in the course of generation, separation, and transport under UV light illumination.

Conclusion

Nanocrystallization process of Ti metal has been achieved by a high-energy shot peening treatment to subdivide bulk crystals into nanocrystallites. Well-aligned TiO_2 nanotube array with an independent tube arrangement and thinned tube walls can be regularly formed on the nanocrystalline Ti substrate by an anodization process. The complex impedance and photoelectrochemical measurements reveal that the charge transfer resistance is obviously decreased and the photocurrent and photovoltage responses are accordingly improved for TiO_2/nanocrystalline Ti nanotube electrode rather than that for TiO_2/bulk crystalline Ti. Such a well-defined TiO_2/Ti nanocomposite with high photoelectron efficiency could potentially act as a promising photoanode for a photoelectric conversion application.

Acknowledgement This study was supported by National Natural Science Foundation of China (No. 20871029), Research Fund for the Doctoral Program of Higher Education of China (No. 200802861071), and Program for New Century Excellent Talents in University.

References

1. Xie YB, Yuan CW (2005) J Mater Sci 40:6375. doi:10.1007/s10853-005-1825-y
2. Yoon JH, Jang SR, Vittal R, Lee J, Kim KJ (2006) J Photochem Photobiol A Chem 180:184
3. Tan B, Wu YY (2006) J Phys Chem B 110:15932
4. Chu SZ, Wada K, Inoue S, Todoroki S (2002) Chem Mater 14:266
5. Xie YB (2006) Electrochim Acta 51:3399
6. Peng XS, Chen AC (2006) Adv Funct Mater 16:1355
7. Wen BM, Liu CY, Liu Y (2005) Chem Lett 34:396
8. Yu XF, Li YX, Ge WY, Yang QB, Zhu NF, Kalantar-Zadeh K (2006) Nanotechnology 17:808
9. Tong WP, Tao NR, Wang ZB, Lu J, Lu K (2003) Science 299:686
10. Tang XH, Li DY (2008) Scr Mater 58:1090
11. Zhang SL, Chen HN, Lin QH (2004) J Mater Sci Technol 20:716
12. Huang L, Lu J, Troyon M (2006) Surf Coat Technol 201:208
13. Yi JH, Bernard C, Variola F, Zalzal SF, Wuest JD, Rosei F, Nanci A (2006) Surf Sci 600:4613
14. Choi JS, Wehrspohn RB, Lee J, Gosele U (2004) Electrochim Acta 49:2645
15. Gong D, Grimes CA, Varghese OK, Hu WC, Singh RS, Chen Z, Dickey EC (2001) J Mater Res 16:3331
16. Ghicov A, Tsuchiya H, Macak JM, Schmuki P (2005) Electrochem Commun 7:505
17. Elsanousi A, Zhang J, Fadlalla HMH, Zhang F, Wang H, Ding XX, Huang ZX, Tang CC (2008) J Mater Sci 43:7219. doi:10.1007/s10853-008-2947-9
18. Jaroenworaluck A, Regonini D, Bowen CR, Stevens R, Allsopp D (2007) J Mater Sci 42:6729. doi:10.1007/s10853-006-1474-9
19. Guo FA, Zhu KY, Trannoy N, Lu J (2004) Thermochimica Acta 419:239
20. Zhu KY, Vassel A, Brisset F, Lu K, Lu J (2004) Acta Mater 52:4101
21. Xie YB (2006) Adv Funct Mater 16:1823
22. He LP, Mai YW, Chen ZZ (2004) Nanotechnology 15:1465
23. Marino CE, de Oliveira EM, Rocha RC, Biaggio SR (2001) Corros Sci 43:1465
24. Macak JM, Tsuchiya H, Schmuki P (2005) Angew Chem Int Ed 44:2100
25. Schmidt T, Martel R, Sandstrom RL, Avouris P (1998) Appl Phys Lett 73:2173
26. Abidian MR, Kim DH, Martin DC (2006) Adv Mater 18:405
27. Marsh J, Gorse D (1998) Electrochim Acta 43:659
28. Yuan S, Hu SS (2004) Electrochim Acta 49:4287
29. Mantzila AG, Prodromidis MI (2006) Electrochim Acta 51:3537
30. Oliva FY, Avalle LB, Santos E, Camara OR (2002) J Photochem Photobiol A Chem 146:175
31. Beranek R, Tsuchiya H, Sugishima T, Macak JM, Taveira L, Fujimoto S, Kisch H, Schmuki P (2005) Appl Phys Lett 87:243114